

# Effect of Different Numbers of $-\text{CH}_2-$ Units on the Performance of Isoquinolinium Dyes

Jianghua Zhao,<sup>†</sup> Xichuan Yang,<sup>\*,†</sup> Yan Hao,<sup>‡</sup> Ming Cheng,<sup>†</sup> Jie Tian,<sup>†</sup> and Licheng Sun<sup>†,§</sup>

<sup>†</sup>State Key Laboratory of Fine Chemicals, DUT–KTH Joint Education and Research Centre on Molecular Devices, Dalian University of Technology (DUT), 2 Linggong Road, 116024 Dalian, China

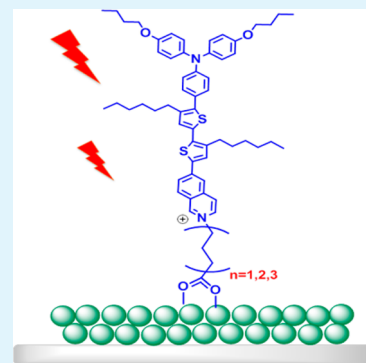
<sup>§</sup>School of Chemical Science and Engineering, Centre of Molecular Devices, Department of Chemistry, KTH Royal Institute of Technology, Teknikringen 30, 10044 Stockholm, Sweden

<sup>‡</sup>Ångström Laboratory, Center of Molecular Devices, Department of Chemistry, Uppsala University, Box 523, 75120 Uppsala, Sweden

## Supporting Information

**ABSTRACT:** Three new dyes have been synthesized to investigate the influence of the distance between the electron acceptor and  $\text{TiO}_2$  surface on the performance of dye-sensitized solar cells (DSSCs). In these dyes, the isoquinolinium acceptor, with a  $-(\text{CH}_2)_n\text{COOH}$  anchoring group, and a functionalized triphenylamine donor are separated by an oligothiophene bridge. The physical and electrochemical properties of the dyes were investigated systematically. The results prove that different numbers of  $-\text{CH}_2-$  units between the isoquinolinium acceptor and the carboxyl anchoring group have a less pronounced effect on the physical and electrochemical properties of these dyes. However, when applied in DSSCs, a sharp decrease in the short-circuit current ( $J_{\text{sc}}$ ) was observed with increasing numbers of  $-\text{CH}_2-$  units. For example, the device containing the organic dye bearing three  $-\text{CH}_2-$  units produced the lowest  $J_{\text{sc}}$  of  $7.94 \text{ mA}\cdot\text{cm}^{-2}$ . In contrast, the device containing the dye bearing only one  $-\text{CH}_2-$  unit exhibited the highest  $J_{\text{sc}}$  of  $13.88 \text{ mA}\cdot\text{cm}^{-2}$ . The higher photocurrent obtained with the device incorporating the dye with one  $-\text{CH}_2-$  unit resulted in a higher power conversion efficiency of 6.8%.

**KEYWORDS:** dye-sensitized solar cells, energy conversion, anchoring group, cationic dyes, isoquinolinium dye, transient absorption



## INTRODUCTION

Donor- $\pi$ -conjugated bridge-acceptor (D- $\pi$ -A)-structured organic dyes frequently used in photon-to-electron conversion systems such as dye-sensitized solar cells (DSSCs)<sup>1–3</sup> and organic solar cells.<sup>4,5</sup> In DSSCs, these types of organic dyes have achieved a photon-to-electron conversion efficiency higher than 10%.<sup>6</sup> Much effort has been devoted to exploring new molecular units; triphenylamine,<sup>7–9</sup> phenoxazine,<sup>10</sup> and indoline<sup>11,12</sup> have been introduced as electron donors successfully; thiophene and its derivatives<sup>13,14</sup> have served as  $\pi$ -conjugated bridges; cyanocrylic acid and rhodanine-N-acetic acid have been widely used as electron acceptors.<sup>15–18</sup> On the basis of such a molecular design, a series of excellent organic dyes have emerged, such as triphenylamine-based C252,<sup>19</sup> Y123,<sup>20</sup> and phenoxazine-based TH305.<sup>21</sup> These dyes exhibit a strong spectral response in the UV–visible region, suitable redox potentials for DSSC applications, and high incident photon-to-electron conversion efficiency (IPCE). Considering the reflection of conducting glass, the IPCE values for DSSC devices based on the dyes above are close to unity in certain regions. There are several explanations for this phenomenon. First, a planar molecule is beneficial for the intramolecular charge-transfer process. Second, a suitable spatial configuration when anchoring on the  $\text{TiO}_2$  surface could facilitate electron

injection from the electron acceptor of the dye into the conduction band ( $E_{\text{cb}}$ )  $\text{TiO}_2$  and suppress electron recombination. Furthermore, the distance between the electron acceptor and  $\text{TiO}_2$  surface could be appropriate for good charge separation, leading to a high efficiency. Therefore, it is worth investigating whether a high efficiency can be maintained when the distance between the electron acceptor and  $\text{TiO}_2$  surface is increased.

Our group reported a series of isoquinolinium photosensitizers, which employed isoquinolinium as the electron acceptor and a carboxyl group as the anchoring group. The highest photon-to-electron conversion efficiency obtained with these dyes was 7.3%.<sup>22</sup> It is difficult to tune the distance between the electron acceptor and  $\text{TiO}_2$  surface for traditional cyanocrylic acid organic dyes. However, the electron acceptor and anchoring group can be easily separated for isoquinolinium dyes by tuning the number of  $-\text{CH}_2-$  units, as shown in Figure 1. In order to explore the impact of the distance between the electron acceptor and  $\text{TiO}_2$  surface on the performance of DSSCs, the series of isoquinolinium photosensitizers with

Received: November 8, 2013

Accepted: February 27, 2014

Published: February 27, 2014

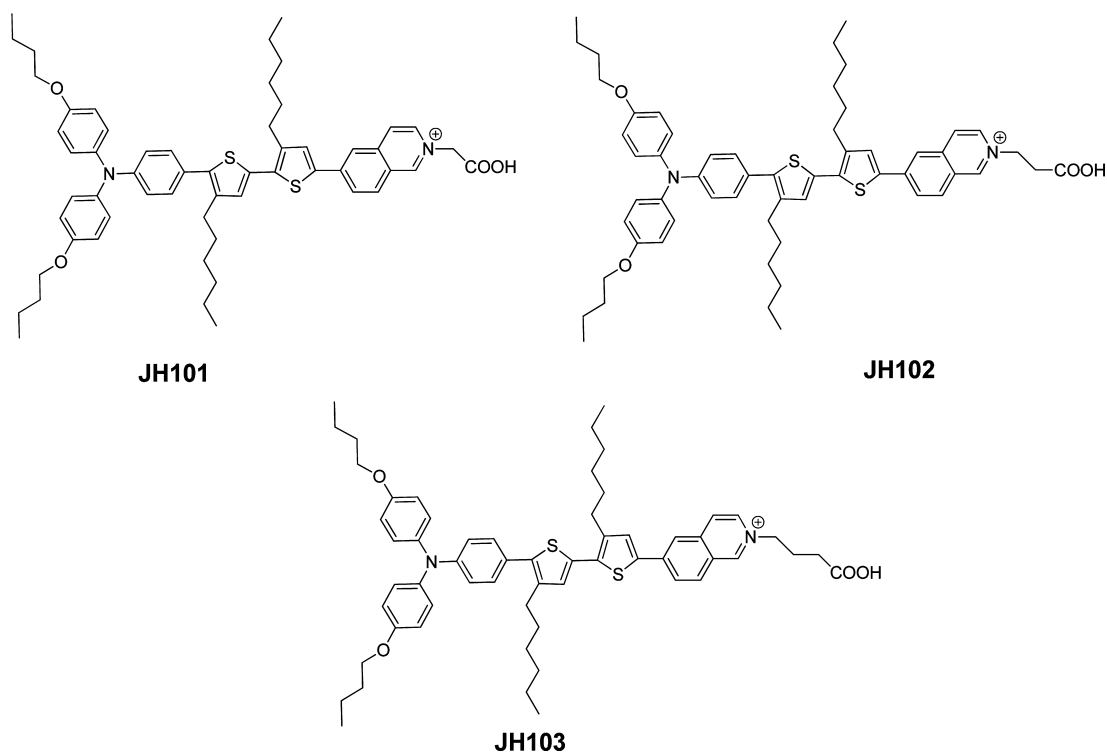


Figure 1. Structures of the sensitizers JH101–JH103.

different numbers of  $-\text{CH}_2-$  units between isoquinolinium and the carboxyl group displayed in Figure 1 have been synthesized and applied in DSSCs. The experimentally determined physical and electrochemical properties of these photosensitizers are also presented.

## EXPERIMENTAL SECTION

**Synthetic Routes.** The synthetic routes of JH101–JH103 are displayed in Figure 2. The solvents used in these reactions were distilled freshly according to standard procedures. The commercial reagents were used as received. The donor and bridge linker were synthesized by our previously reported procedure.<sup>22</sup> The structures of the compounds were identified by  $^1\text{H}$  NMR and mass spectrometry (MS). The  $^1\text{H}$  NMR spectra of the final product are shown in Figure S2 in Supporting Information (SI).

**General Synthetic Procedures.** 6-(3,4'-Dihexyl-2,2'-bithiophen-5-yl)isoquinoline (1). 6-Bromoisquinoline (1 g, 4.83 mmol), 2-(3,4'-dihexyl-2,2'-bithiophen-5-yl)-4,4,5,5-tetramethyl-1,3,2-dioxaborolane (2.67 g, 5.8 mmol),  $\text{K}_2\text{CO}_3$  (1.29 g, 7.25 mmol), and  $\text{Pd}(\text{PPh}_3)_4$  (48 mg) were dissolved in tetrahydrofuran (THF)/ $\text{H}_2\text{O}$  (5:1, v/v) under  $\text{N}_2$ . The mixture was refluxed for 12 h. Then the reaction was cooled to the room temperature, and water was added and extracted with  $\text{CH}_2\text{Cl}_2$ . The combined organic phase was dried over anhydrous  $\text{MgSO}_4$ , and the solvent was removed by rotary evaporation. The crude product was purified by  $\text{CH}_2\text{Cl}_2$  to give compound 1 (1.74 g, 68%) as a yellow oil.  $^1\text{H}$  NMR (400 MHz,  $\text{CDCl}_3$ ):  $\delta$  9.20 (s, 1H), 8.50 (d,  $J = 5.7$  Hz, 1H), 8.02–7.89 (m, 2H), 7.84 (d,  $J = 8.6$  Hz, 1H), 7.64 (t,  $J = 9.2$  Hz, 1H), 7.34 (d,  $J = 3.1$  Hz, 1H), 7.01 (s, 1H), 6.93 (s, 1H), 2.87–2.73 (m, 2H), 2.63 (dd,  $J = 15.5, 7.8$  Hz, 2H), 1.84–1.55 (m, 4H), 1.51–1.16 (m, 12H), 0.90 (dd,  $J = 6.4$  and 5.6 Hz, 6H). MS ( $m/z$ ):  $[\text{M}]^+$  calcd for  $\text{C}_{29}\text{H}_{35}\text{NSO}_2$ , 461.2211; found, 461.2232.

6-(5'-Bromo-3,4'-dihexyl-2,2'-bithiophen-5-yl)isoquinoline (2). Compound 1 (1.02 g, 2.23 mmol) was dissolved in THF at 0  $^\circ\text{C}$ , *N*-bromosuccinimide (NBS; 416 mg, 2.34 mmol) was added slowly, and the resulting mixture was stirred for 3 h. When the reaction was finished, water was added and the mixture was extracted with  $\text{CH}_2\text{Cl}_2$ . The organic layer was collected and concentrated by rotary evaporation. The crude product was purified by  $\text{CH}_2\text{Cl}_2$  to give

compound 2 (1.12 g, 94%) as a yellow oil.  $^1\text{H}$  NMR (400 MHz,  $\text{CDCl}_3$ ):  $\delta$  9.25 (s, 1H), 8.51 (d,  $J = 5.5$  Hz, 1H), 8.01 (d,  $J = 8.7$  Hz, 2H), 7.95–7.86 (m, 1H), 7.71 (t,  $J = 5.4$  Hz, 1H), 7.37 (d,  $J = 7.6$  Hz, 1H), 7.06 (s, 1H), 6.89 (s, 1H), 2.86–2.73 (m, 2H), 2.66–2.52 (m, 2H), 1.80–1.56 (m, 4H), 1.47–1.27 (m, 12H), 0.90 (t,  $J = 5.8$  Hz, 6H). MS ( $m/z$ ):  $[\text{M}]^+$  calcd for  $\text{C}_{29}\text{H}_{34}\text{NBrS}_2$ , 539.1316; found, 539.1313.

4-Butoxy-*N*-(4-butoxyphenyl)-*N*-[4-(3',4'-dihexyl-5'-isoquinolin-6-yl-2,2'-bithiophen-5-yl)phenyl]aniline (3). Compound 1 (1 g, 1.86 mmol), [4-[bis(4-butoxyphenyl)amino]phenyl]boronic acid (0.96 g, 2.23 mmol),  $\text{K}_2\text{CO}_3$  (385 mg, 2.79 mmol), and  $\text{Pd}(\text{PPh}_3)_4$  (19 mg) were dissolved in THF/ $\text{H}_2\text{O}$  (5:1, v/v) under  $\text{N}_2$ . The mixture was refluxed for 12 h. Then the reaction was cooled to the room temperature, and water was added and extracted by  $\text{CH}_2\text{Cl}_2$ . The combined organic phase was dried over anhydrous  $\text{MgSO}_4$ , and the solvent was removed by rotary evaporation. The crude product was purified by silica gel column chromatography with  $\text{CH}_2\text{Cl}_2$ /methanol (50:1) to give compound 3 (1.13 g, 72%) as an orange oil.  $^1\text{H}$  NMR (400 MHz,  $\text{CDCl}_3$ ):  $\delta$  9.22 (s, 1H), 8.50 (d,  $J = 5.7$  Hz, 1H), 8.02–7.94 (m, 2H), 7.89 (d,  $J = 11.9$  Hz, 1H), 7.69 (d,  $J = 5.7$  Hz, 2H), 7.45 (dd,  $J = 16.1$  and 10.7 Hz, 1H), 7.30–7.22 (m, 3H), 7.17–7.03 (m, 5H), 6.94 (d,  $J = 8.5$  Hz, 2H), 6.85 (m, 3H), 3.95 (t,  $J = 6.5$  Hz, 4H), 2.68 (ddd,  $J = 31.9, 20.1$ , and 11.9 Hz, 4H), 1.75 (ddd,  $J = 18.8, 13.7$ , and 6.5 Hz, 4H), 1.49 (m, 8H), 1.38–1.20 (m, 12H), 1.03–0.86 (dt,  $J = 27.2$  and 12.6 Hz, 12H). MS ( $m/z$ ):  $[\text{M}]^+$  calcd for  $\text{C}_{55}\text{H}_{64}\text{N}_2\text{O}_2\text{S}_2$ , 848.4409; found, 848.4504.

6-[5'-[4-[bis(4-butoxyphenyl)amino]phenyl]-3,4'-dihexyl-2,2'-bithiophen-5-yl]-2-(2-ethoxy-2-oxoethyl)isoquinolin-2-ium (4). Compound 3 (200 mg, 0.24 mmol) and  $\text{BrCH}_2\text{COOCH}_2\text{CH}_3$  (197 mg, 1.2 mmol) were dissolved in a  $\text{CH}_3\text{CN}$  solution and refluxed for 5 h. When the reaction was finished, water was added and the mixture was extracted with  $\text{CH}_2\text{Cl}_2$ . The organic layer was collected and concentrated by rotary evaporation. The crude product was purified by  $\text{CH}_2\text{Cl}_2$ / $\text{CH}_3\text{OH}$  (8:1) to give compound 4 (195 mg, 87%) as a red solid.  $^1\text{H}$  NMR (400 MHz, DMSO):  $\delta$  9.86 (s, 1H), 8.66 (d,  $J = 6.2$  Hz, 1H), 8.54 (d,  $J = 8.7$  Hz, 1H), 8.51–8.45 (m, 1H), 8.42 (d,  $J = 8.5$  Hz, 1H), 8.02 (d,  $J = 8.0$  Hz, 1H), 7.26 (d,  $J = 8.7$  Hz, 2H), 7.22 (s, 1H), 7.06–7.02 (m, 2H), 6.93 (d,  $J = 8.9$  Hz, 4H), 6.79 (d,  $J = 8.6$  Hz, 2H), 6.60 (d,  $J = 7.1$  Hz, 2H), 5.74 (s, 2H), 4.12–3.95 (m, 6H), 2.69–

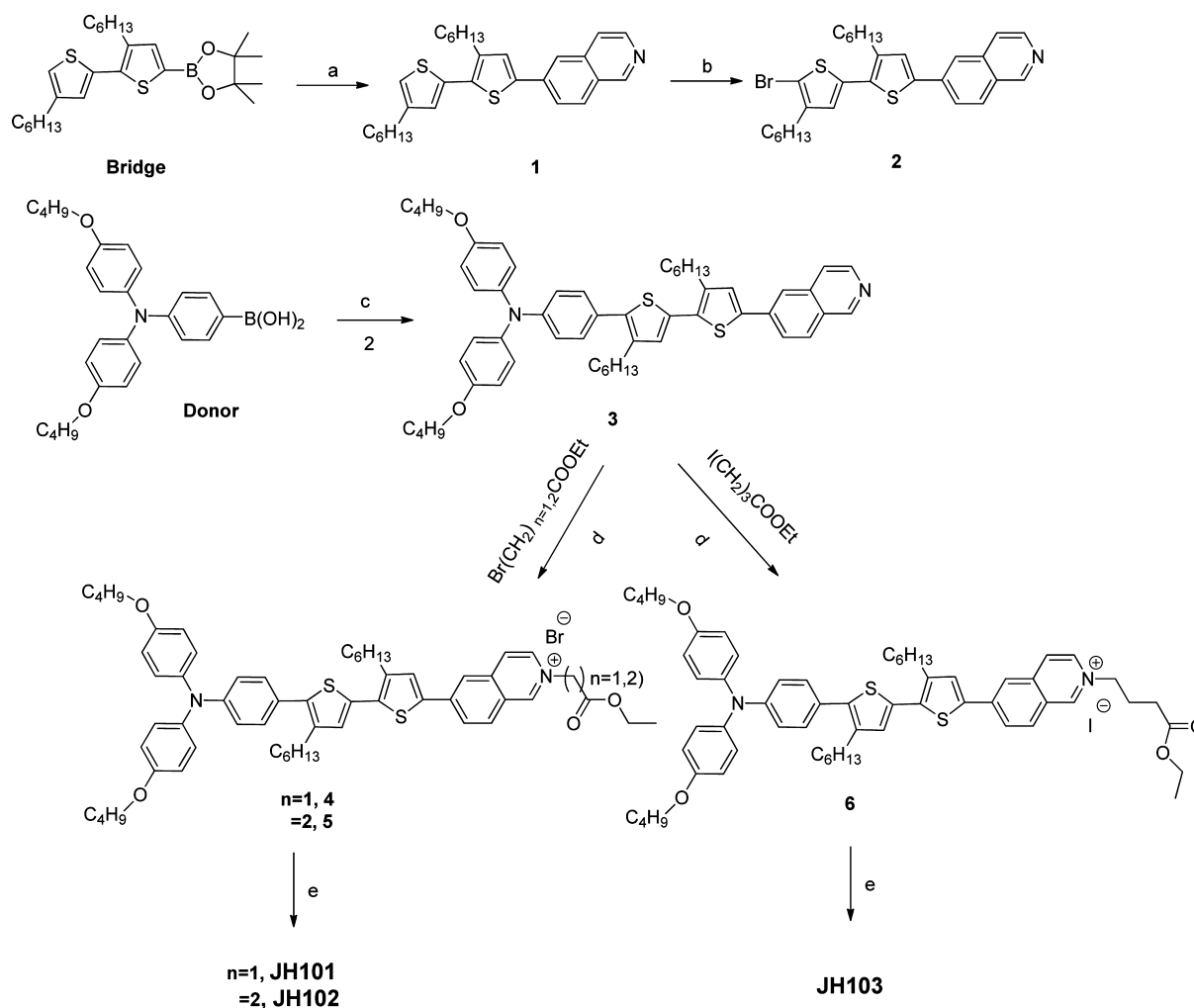


**Figure 2.** Synthetic routes of JH101–JH103: (a)  $\text{K}_2\text{CO}_3$ ,  $\text{Pd}(\text{PPh}_3)_4$ , 6-bromisoquinoline, THF/ $\text{H}_2\text{O}$ , reflux, 12 h; (b) NBS, THF, 0 °C, 3 h; (c)  $\text{K}_2\text{CO}_3$ ,  $\text{Pd}(\text{pPh}_3)_4$ , THF/ $\text{H}_2\text{O}$ , reflux, 12 h; (d) acetonitrile, reflux, 12 h; (e)  $\text{LiOH}\cdot\text{H}_2\text{O}$ ,  $\text{CH}_2\text{Cl}_2/\text{EtOH}/\text{H}_2\text{O}$ , room temperature, 24 h.

2.59 (m, 4H), 1.74–1.64 (m, 4H), 1.48–1.36 (m, 8H), 1.35–1.19 (m, 14H), 0.89 (dt,  $J = 38.9$  and  $7.1$  Hz, 15H). MS ( $m/z$ ):  $[\text{M}]^+$  calcd for  $\text{C}_{59}\text{H}_{71}\text{N}_2\text{O}_4\text{S}_2$ , 935.4855; found, 935.4838.

6-[5'-[4-[bis(4-butoxyphenyl)amino]phenyl]-3,4'-dihexyl-2,2'-bithiophen-5-yl]-2-(3-ethoxy-3-oxopropyl)isoquinolin-2-ium (5). Compound 3 (200 mg, 0.24 mmol) and  $\text{BrCH}_2\text{CH}_2\text{COOCH}_2\text{CH}_3$  (217 mg, 1.2 mmol) were dissolved in a  $\text{CH}_3\text{CN}$  solution and refluxed for 12 h. After the reaction was finished, water was added and the mixture was extracted with  $\text{CH}_2\text{Cl}_2$  and concentrated by rotary evaporation. The crude product was purified by  $\text{CH}_2\text{Cl}_2/\text{CH}_3\text{OH}$  (8:1) to give compound 5 (187 mg, 82%) as a red solid.  $^1\text{H}$  NMR (400 MHz, DMSO):  $\delta$  9.93 (s, 1H), 8.73 (d,  $J = 6.7$  Hz, 1H), 8.53 (s, 1H), 8.46 (d,  $J = 7.6$  Hz, 2H), 7.98 (s, 1H), 7.27 (d,  $J = 8.7$  Hz, 2H), 7.08 (m, 2H), 6.95 (d,  $J = 8.7$  Hz, 2H), 6.92 (d,  $J = 3.5$  Hz, 2H), 6.80 (m, 4H), 6.60 (d,  $J = 7.1$  Hz, 2H), 5.75 (s, 1H), 4.07 (dd,  $J = 14.2$  and  $7.1$  Hz, 2H), 3.95 (t,  $J = 6.4$  Hz, 6H), 2.85 (t,  $J = 6.4$  Hz, 4H), 1.69 (dd,  $J = 14.4$  and  $6.5$  Hz, 4H), 1.48–1.37 (m, 8H), 1.25 (d,  $J = 9.6$  Hz, 16H), 0.97–0.81 (m, 15H). MS ( $m/z$ ):  $[\text{M}]^+$  calcd for  $\text{C}_{60}\text{H}_{73}\text{N}_2\text{O}_4\text{S}_2$ , 949.5006; found, 949.2892.

6-[5'-[4-[bis(4-butoxyphenyl)amino]phenyl]-3,4'-dihexyl-2,2'-bithiophen-5-yl]-2-(3-ethoxy-3-oxopropyl)isoquinolin-2-ium (6). Compound 3 (200 mg, 0.24 mmol) and  $\text{ICH}_2\text{CH}_2\text{CH}_2\text{COOCH}_2\text{CH}_3$  (480 mg, 2.4 mmol) were dissolved in a  $\text{CH}_3\text{CN}$  solution and refluxed for 24 h. After the reaction was finished, water was added and the mixture was extracted with  $\text{CH}_2\text{Cl}_2$  and concentrated by rotary evaporation. The crude product was purified by  $\text{CH}_2\text{Cl}_2/\text{CH}_3\text{OH}$  (8:1) to give compound 6 (110 mg, 48%) as a red solid.  $^1\text{H}$  NMR (400 MHz,  $\text{CDCl}_3$ ):  $\delta$  10.15 (d,  $J = 9.6$  Hz, 1H), 8.61 (d,  $J = 8.8$  Hz,

1H), 8.43 (d,  $J = 6.3$  Hz, 1H), 8.19–8.06 (m, 3H), 7.26–7.21 (m, 2H), 7.11 (d,  $J = 2.8$  Hz, 2H), 7.09 (s, 1H), 7.00 (s, 1H), 6.94 (d,  $J = 8.7$  Hz, 2H), 6.85 (d,  $J = 8.9$  Hz, 4H), 6.73 (d,  $J = 8.8$  Hz, 2H), 5.05 (t,  $J = 7.7$  Hz, 2H), 3.95 (t,  $J = 6.5$  Hz, 6H), 2.70–2.60 (t, 4H), 2.50–2.41 (m, 2H), 1.81–1.72 (m, 6H), 1.50 (dd,  $J = 15.0$  and  $7.5$  Hz, 8H), 1.32–1.22 (m, 16H), 0.99–0.85 (m, 15H). MS ( $m/z$ ): calcd for  $\text{C}_{61}\text{H}_{75}\text{N}_2\text{O}_4\text{S}_2$ , 963.5168; found, 963.5131.

6-[5'-[4-[bis(4-butoxyphenyl)amino]phenyl]-3,4'-dihexyl-2,2'-bithiophen-5-yl]-2-(carboxymethyl)isoquinolin-2-ium (JH101). Compound 4 (190 mg, 0.2 mmol) and  $\text{LiOH}\cdot\text{H}_2\text{O}$  (84 mg, 2 mmol) were dissolved in  $\text{CH}_2\text{Cl}_2/\text{EtOH}/\text{H}_2\text{O}$  (1:2:0.02). The mixture was stirred at room temperature for 24 h. When the reaction was finished, 2 M HCl was added to adjust the pH to neutral. Then the mixture was extracted with  $\text{CH}_2\text{Cl}_2$  and evaporated to dryness. The crude red solid was purified by silica gel column chromatography with  $\text{CH}_2\text{Cl}_2/\text{CH}_3\text{OH}$  (5:1, v/v) to give a red solid (58 mg, 32%).  $^1\text{H}$  NMR (400 MHz, DMSO- $d_6$ ):  $\delta$  10.21 (s, 1H), 9.69 (s, 1H), 8.50 (d, 1H), 8.43–8.36 (d, 2H), 7.96 (d, 1H), 7.31–7.27 (d,  $J = 8.9$  Hz, 2H), 7.22–7.13 (s, 1H), 7.08 (d,  $J = 8.8$  Hz, 2H), 6.94 (d,  $J = 8.7$  Hz, 4H), 6.79 (d,  $J = 8.5$  Hz, 4H), 6.61 (d, 2H), 4.95 (s, 2H), 4.22–3.95 (m, 4H), 2.65–2.33 (m, 4H), 1.70 (m, 4H), 1.44 (dd,  $J = 14.8$  and  $7.4$  Hz, 8H), 1.26 (d,  $J = 22.2$  Hz, 16H), 0.97–0.79 (m, 12H).  $^{13}\text{C}$  NMR (101 MHz,  $\text{CDCl}_3$ ):  $\delta$  155.65, 148.32, 147.14, 140.31, 131.41, 129.11, 126.81, 119.62, 115.26, 67.89, 65.58, 31.54, 30.95, 29.71, 29.37, 22.65, 19.29, 18.82, 14.13, 13.80. MS ( $m/z$ ):  $[\text{M}]^+$  calcd for  $\text{C}_{57}\text{H}_{67}\text{N}_2\text{O}_4\text{S}_2$ , 907.4537; found, 907.4532.

6-[5'-[4-[bis(4-butoxyphenyl)amino]phenyl]-3,4'-dihexyl-2,2'-bithiophen-5-yl]-2-(carboxymethyl)isoquinolin-2-ium (JH102). A syn-

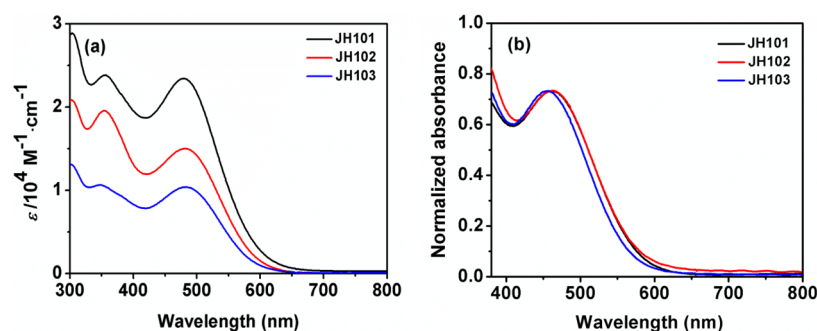


Figure 3. Absorption spectra of JH101–JH103 in a CH<sub>2</sub>Cl<sub>2</sub> solution (a) and on a TiO<sub>2</sub> film (b).

Table 1. Absorption and Electrochemical Data of JH101–JH103

dye	$\lambda_{\text{max}}$ (nm)	$\epsilon$ at $\lambda_{\text{max}}$ ( $\text{M}^{-1} \cdot \text{cm}^{-1}$ )	$\lambda_{\text{max}}$ <sup>a</sup> on the film (nm)	$E_{0-0}$ <sup>b</sup> (V)	$E_{\text{HOMO}}$ <sup>c</sup> (V vs NHE)	$E_{\text{LUMO}}$ (V vs NHE)
JH101	481	23400	464	2.16	0.62	−1.54
JH102	481	14900	463	2.16	0.62	−1.54
JH103	479	10400	456	2.19	0.64	−1.55

<sup>a</sup>Absorption spectra on the TiO<sub>2</sub> film were measured with a dye-loaded TiO<sub>2</sub> film immersed in a CH<sub>2</sub>Cl<sub>2</sub> solution. <sup>b</sup> $E_{0-0}$  was determined from the intersection of the tangent of absorption on the TiO<sub>2</sub> film and the x axis by  $1240/\lambda$ . <sup>c</sup>The oxidation potentials of the dyes were measured in a CH<sub>2</sub>Cl<sub>2</sub> solution with TBAPF<sub>6</sub> (0.1 M) as an electrolyte and ferrocene/ferrocenium ( $F_c/F_c^+$ ) as an internal reference and converted to NHE by the addition of 440 mV.

thetic procedure similar to that of JH101 was used to give JH102 as a red solid (49 mg, 28%). <sup>1</sup>H NMR (400 MHz, DMSO-*d*<sub>6</sub>):  $\delta$  10.08 (s, 1H), 9.63 (s, 1H), 8.43 (d, 2H), 8.27 (d, 1H), 8.12 (d, *J* = 12.7 Hz, 1H), 7.97 (s, 1H), 7.20 (d, *J* = 8.1 Hz, 2H), 7.15 (s, 1H), 7.05 (d, *J* = 8.9 Hz, 2H), 6.87 (d, *J* = 8.7 Hz, 4H), 6.81 (d, *J* = 8.2 Hz, 4H), 6.47 (t, *J* = 5.2 Hz, 2H), 4.92 (t, 2H), 4.93 (t, 2H), 3.94 (t, *J* = 6.1 Hz, 4H), 2.68–2.56 (m, 4H), 2.32 (t, 2H), 1.70 (d, *J* = 6.7 Hz, 4H), 1.46 (dd, *J* = 14.8 and 7.6 Hz, 8H), 1.35–1.19 (m, 16H), 1.00–0.77 (m, 12H). <sup>13</sup>C NMR (101 MHz, DMSO-*d*<sub>6</sub>):  $\delta$  155.65, 148.32, 147.14, 140.31, 131.41, 129.11, 126.81, 119.62, 115.26, 67.89, 65.58, 31.54, 30.95, 29.71, 29.37, 23.1, 22.65, 19.29, 18.82, 14.13, 13.80. MS (*m/z*): [ $M$ ]<sup>+</sup> calcd for C<sub>58</sub>H<sub>69</sub>N<sub>2</sub>O<sub>4</sub>S<sub>2</sub>, 921.4693; found, 921.4115.

6-[5'-[4-[bis(4-butoxyphenyl)amino]phenyl]-3,4'-dihexyl-2,2'-bi-thiophen-5-yl]-2-(3-carboxypropyl)isoquinolin-2-ium (JH103). A synthetic procedure similar to that of JH101 was used to give JH103 as a red solid (12 mg, 12%). <sup>1</sup>H NMR (400 MHz, DMSO-*d*<sub>6</sub>):  $\delta$  9.97 (s, 1H), 9.58 (s, 1H), 8.73 (d, *J* = 6.8 Hz, 2H), 8.46 (d, *J* = 8.3 Hz, 1H), 8.39 (s, 1H), 7.94 (s, 1H), 7.25 (d, *J* = 8.6 Hz, 2H), 7.19 (s, 1H), 7.07 (d, *J* = 8.7 Hz, 2H), 6.92 (d, *J* = 8.9 Hz, 4H), 6.81 (d, *J* = 8.6 Hz, 4H), 6.52 (d, *J* = 5.0 Hz, 2H), 4.71 (t, 3H), 3.95 (t, *J* = 6.2 Hz, 6H), 2.70–2.58 (m, 4H), 2.35–2.20 (m, 2H), 1.76–1.56 (m, 6H), 1.44–1.33 (m, 8H), 1.04–0.80 (m, 12H). MS (*m/z*): [ $M$ ]<sup>+</sup> calcd for C<sub>59</sub>H<sub>71</sub>N<sub>2</sub>O<sub>4</sub>S<sub>2</sub>, 935.4850; found, 935.4153.

**Preparation of the DSSCs.** The DSSCs sensitized by JH101–JH103 were fabricated as reported previously.<sup>23</sup> Briefly, 20-nm-sized TiO<sub>2</sub> paste was coated on the fluorine-doped tin oxide conductive glass by screen printing five times (10 nm). A 200–300-nm-sized scattering layer was then coated on top. After that, the electrode was heated at 520 °C for 45 min and then cooled to room temperature. The sintered TiO<sub>2</sub> film was further treated with a 40 mM TiCl<sub>4</sub> aqueous solution at 70 °C for 30 min and annealed at 520 °C for 45 min again to improve the quality of the surface. After that, the TiO<sub>2</sub> film was immersed in a  $2 \times 10^{-4}$  M dye bath containing saturated chenodeoxycholic acid (CDCA) for 12 h. Then the sensitized TiO<sub>2</sub> electrode and platinum-coated conductive glass was compacted and separated with a hot-melt film. The TiO<sub>2</sub> films used for UV–visible absorption measurements were prepared by depositing a 2- $\mu\text{m}$ -thick layer of TiO<sub>2</sub> paste on a glass slide by a doctor blade and sintered at 520 °C for 45 min.

**Analytical Instruments.** The photocurrent–voltage (*J*–*V*) properties were measured under AM 1.5G illumination (16S-002, Solar Light Co. Ltd., USA). The incident light intensity was 100 mW·cm<sup>−2</sup> calibrated with a standard silicon solar cell. The working area of

the device was masked to 0.159 cm<sup>2</sup>. The *J*–*V* data were collected by an electrochemical workstation (LK9805, Lanlike Co. Ltd., China). Measurement of the IPCE was obtained by a Hypermono light (SM-25, Jasco Co. Ltd., Japan). Electrochemical impedance spectroscopy (EIS) was measured with an impedance/gain-phase analyzer (PARSTAT 2273, USA) in the dark, with a forward bias of −0.7 V. The alternating-current amplitude was set at 10 mV. Nanosecond time-resolved transient absorption (TA) spectra were recorded on a LP 920 laser flash photolysis spectrometer (Edinburgh Instruments, Livingston, U.K.). The samples were excited with a 532 nm laser, and the transient signals were recorded on a Tektronix TDS 3012B oscilloscope.

## RESULTS AND DISCUSSION

**Physical and Electrochemical Properties.** UV–visible absorption spectra of JH101–JH103 in a CH<sub>2</sub>Cl<sub>2</sub> solution and on a TiO<sub>2</sub> film are displayed in Figure 3, and the corresponding physical data are listed in Table 1. The concentrations of the dyes are  $2 \times 10^{-5}$  M. In Figure 3a, two main absorption bands for JH101–JH103 can be observed. The absorption bands in the higher energy region (330 nm) are assigned to a  $\pi \rightarrow \pi^*$  transition. The absorption bands in the lower energy region (around 480 nm) correspond to the  $S_0 \rightarrow S_1$  transition. There was no obvious effect on the absorption maxima for either band when the number of −CH<sub>2</sub>− units was changed. This is due to the weak inductive effect of the −CH<sub>2</sub>− units on the electron acceptor. The molar extinction coefficients tend to decrease with an increase of the −CH<sub>2</sub>− units for JH101–JH103. In a CH<sub>2</sub>Cl<sub>2</sub> solution, there is an equilibrium between dyes with protonated and deprotonated carboxyl groups.<sup>24</sup> For JH101–JH103, as the number of −CH<sub>2</sub>− units is increased, the isoquinolinium cationic center and anionic carboxyl group are separated. This change in the interaction between the dyes and solvent may be responsible for the change in the molar extinction coefficients.

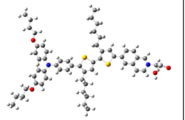
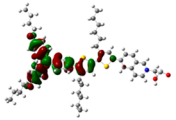
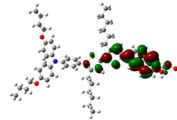
Figure 3b shows the normalized absorption spectra of JH101–JH103 anchored on a TiO<sub>2</sub> film. The spectra are similar for JH101–JH103, with absorption maxima at 464, 463, and 456 nm for dyes JH101–JH103, respectively. Compared

to the absorption spectra in solution, a hypsochromic shift was observed for **JH101**–**JH103** upon adsorption on  $\text{TiO}_2$  from a  $\text{CH}_2\text{Cl}_2$  solution. This hypsochromic shift has been observed for many D– $\pi$ –A organic dyes and can be mainly attributed to the formation of H-type aggregation.<sup>25–27</sup>

Cyclic voltammetry was employed to study the electrochemical properties of **JH101**–**JH103**. The curves are collected in the SI (see Figure S1), and the corresponding data are depicted in Table 1. The highest occupied molecular orbital (HOMO) levels of all of the dyes are more positive than  $\text{I}^-/\text{I}_3^-$  (0.4 V vs NHE),<sup>28</sup> indicating that the oxidized dyes can be regenerated effectively by the electrolyte. The lowest unoccupied molecular orbital (LUMO) levels of **JH101**–**JH103** are all more negative than  $E_{\text{cb}}$  of  $\text{TiO}_2$  (–0.5 V vs NHE),<sup>29</sup> implying that the excited dyes can inject an electron into the  $\text{TiO}_2$  conduction band thermodynamically. It is also noticeable that the HOMO and LUMO values for **JH101**–**JH103** are almost identical. We can summarize that the number of  $-\text{CH}_2-$  units between isoquinolinium and the carboxyl group has a less pronounced effect on the physical and electrochemical properties.

Because there was no obvious variation in the electrochemical properties for the **JH** series of dyes, **JH101** was chosen to study the electronic distribution of the dyes. The ground-state-optimized geometry of **JH101** was obtained using density functional theory (DFT) calculation at the B3LYP/6-31G level. The results are shown in Table 2. The HOMO levels

**Table 2. Optimized Structures and Electron Distribution in the HOMO and LUMO Levels of JH101**

Dye	Optimized structure	HOMO	LUMO
<b>JH101</b>			

of each of the dyes are distributed along the  $\pi$  system covering the electron donor and part of the spacer. The LUMO levels of the dyes are mainly concentrated at the isoquinolinium motif and part of the spacer.

**Photovoltaic Performance.** The current density–voltage properties of the DSSCs based on **JH101**–**JH103** were evaluated under standard AM 1.5G illumination. The  $J$ – $V$  curves and photovoltaic parameters are presented in Figure 4

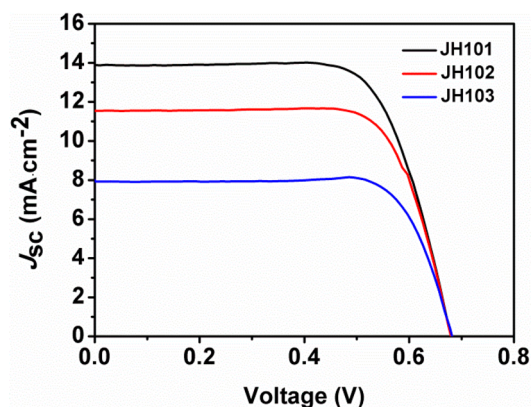


**Figure 4.**  $J$ – $V$  curves of the device sensitized with **JH101**–**JH103**.

and Table 3. The DSSCs sensitized with **JH101** clearly exhibit the highest photon-to-electron conversion efficiency ( $\eta$ ) of

**Table 3. Photovoltaic Performance<sup>a</sup> of DSSCs Based on the JH Series of Dyes**

dye <sup>b</sup>	$J_{\text{sc}}$ ( $\text{mA}\cdot\text{cm}^{-2}$ )	$V_{\text{oc}}$ (mV)	FF (%)	$\eta$ (%)
<b>JH101</b>	13.88	679	71.2	6.8
<b>JH102</b>	11.55	679	74.1	5.8
<b>JH103</b>	7.94	682	77.3	4.2

<sup>a</sup>Irradiation light: AM 1.5G simulated solar light at room temperature; working area, 0.159  $\text{cm}^2$ , electrolyte, 0.6 M DMPII, 0.06 M LiI, 0.4 M 4-*tert*-butylpyridine, and 0.02 M  $\text{I}_2$  in dry acetonitrile. <sup>b</sup>The electrodes were sensitized with **JH101**–**JH103** in  $2 \times 10^{-4}$  M solution in  $\text{CH}_2\text{Cl}_2$ . The average error was less than 5%.

6.8%, with  $J_{\text{sc}}$  of 13.88  $\text{mA}\cdot\text{cm}^{-2}$ ,  $V_{\text{oc}}$  of 679 mV, and a fill factor (FF) of 74.9%. As the  $-\text{CH}_2-$  units are increased for **JH102** and **JH103**,  $J_{\text{sc}}$  of the devices decreased sharply. One explanation for this trend is a decrease in the ability to inject an electron into  $\text{TiO}_2$ , as described by Durrant et al.<sup>30</sup> When the LUMO orbitals of the dyes are further away from the  $\text{TiO}_2$  surface, the injection could be slower. Although **JH101**–**JH103** exhibit a similar thermodynamic driving force for charge transfer, a nonconjugated alkyl spacer separates the electron acceptor and carboxyl anchoring group. Increasing the number of  $-\text{CH}_2-$  units may increase the distance between the LUMO orbital of the dye and the surface of  $\text{TiO}_2$  and hinder electron injection. We can conclude that a short distance between the electron acceptor and  $\text{TiO}_2$  surface is advantageous for improvement of the photon-to-current conversion efficiency for **JH101**–**JH103**. It is therefore perhaps encouraging to find that dye **JH103** with three  $-\text{CH}_2-$  units can still achieve a device efficiency of 4.2%.

The IPCE spectra of **JH101**–**JH103** are displayed in Figure 5.  $\text{IPCE}(\lambda) = \text{LHE}(\lambda) \phi_{\text{inj}} \eta_{\text{C}}$ ,<sup>31</sup> where  $\phi_{\text{inj}}$  is the quantum yield

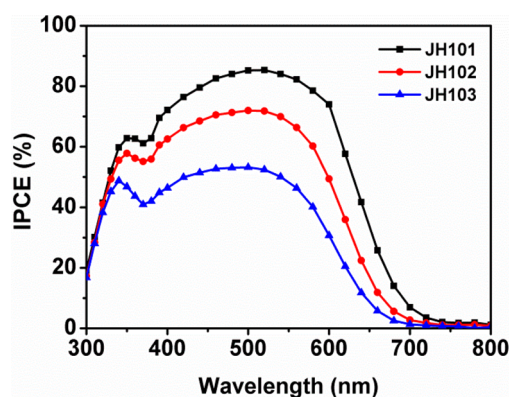


**Figure 5.** IPCE curves for DSSCs containing **JH101**–**JH103**.

of electron injection. Figure 5 shows that the IPCE response in the visible region decreases with an increase of the  $-\text{CH}_2-$  units for **JH101**–**JH103** sensitized devices, in agreement with the trend for  $J_{\text{sc}}$  for **JH101**–**JH103** described above. The device containing **JH101** exhibited the best incident photon-to-electron conversion ability with a maximum IPCE value of 85% at around 500 nm in comparison with 72% and 53% for the **JH102**- and **JH103**-based devices, respectively.

To evaluate interfacial charge-transfer processes in the DSSCs containing **JH101**–**JH103**, EIS was employed.<sup>32</sup> Figure

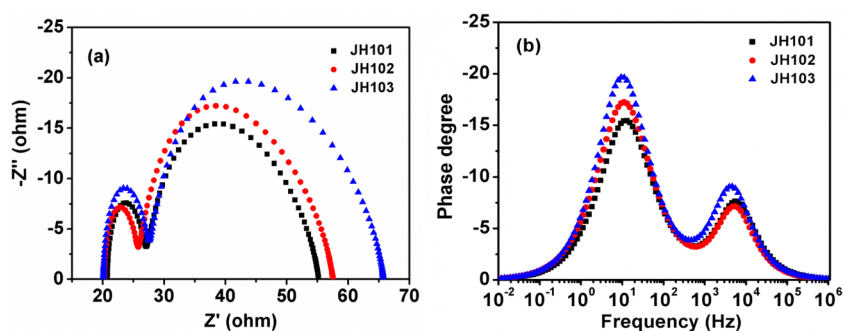


Figure 6. Nyquist (a) and Bode (b) plots of DSSCs based on JH101–JH103.

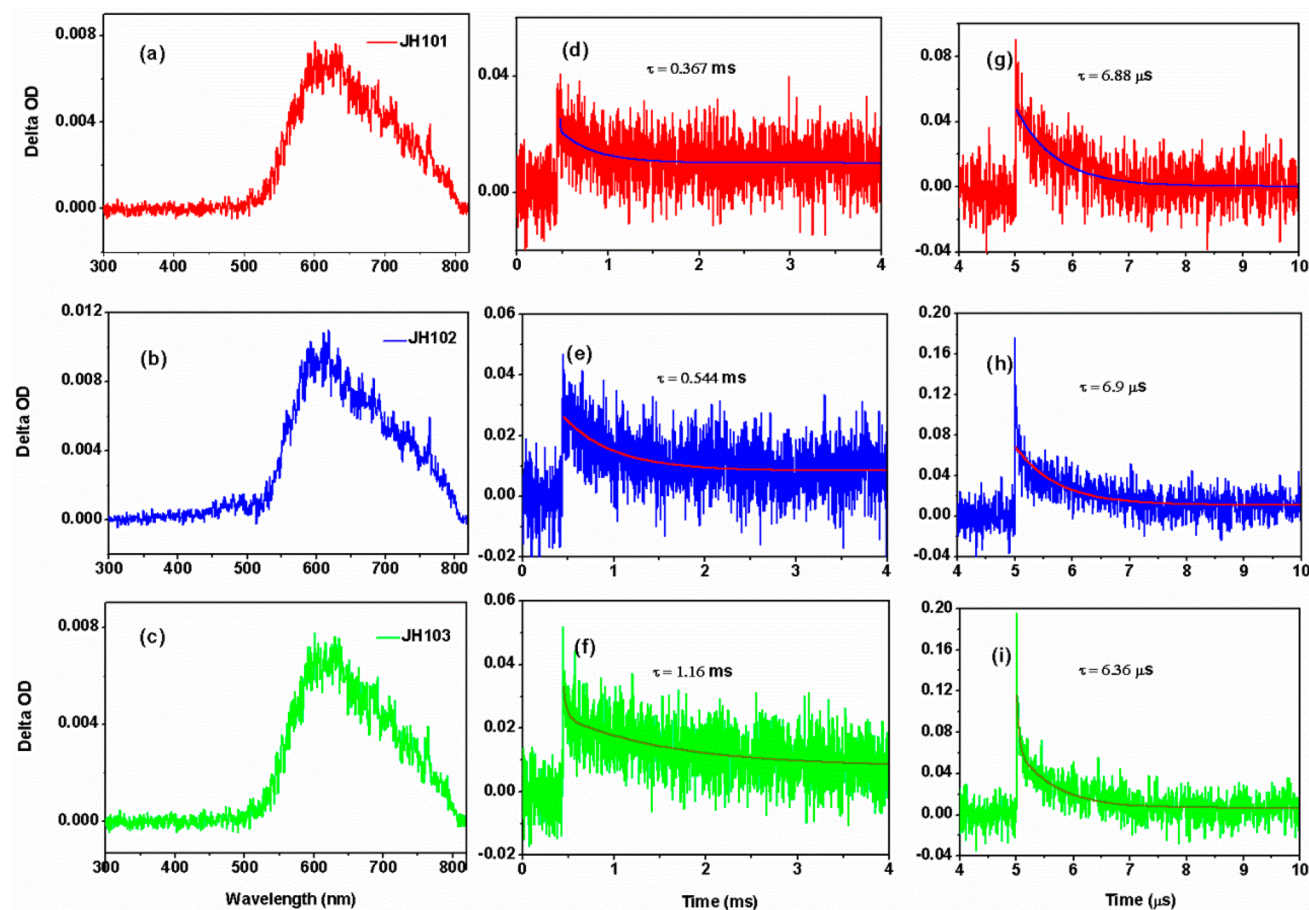


Figure 7. TA of dyes JH101–JH103 (a–c) under a 532 nm laser pulse. Kinetic absorption traces of both dyes were monitored under a 532 nm laser pulse of a 10- $\mu\text{m}$ -thick  $\text{TiO}_2$  film permeated with (d–f) inert electrolyte A and (g–i) electrolyte B.

6a shows the Nyquist plots; the high-frequency region ( $10^5$ – $10^6$  Hz) represents the series resistance ( $R_s$ ), corresponding to the diameter value of the first semicircle; the larger semicircle in the mid-frequency region ( $10^4$ – $10^5$  Hz) reflects the recombination resistance ( $R_{ct}$ ) at the  $\text{TiO}_2$ /dye/electrolyte interface.  $R_{ct}$  values of 29.4, 30.5, and 38.1  $\Omega\cdot\text{cm}^{-2}$  were obtained for the JH101–JH103-based devices, respectively. Charge recombination at the  $\text{TiO}_2$  surface can occur between the injected electrons with the oxidized dye molecules ( $\text{dye}^+$ ) and with oxidized species in the electrolyte. When the number of  $-\text{CH}_2-$  units is increased, the positions of the  $\text{dye}^+$  are away from the surface of  $\text{TiO}_2$ , which could hinder recombination. We can conclude that increasing the number of  $-\text{CH}_2-$  groups is beneficial to restricting electron recombination, resulting in a

larger recombination resistance; the smaller semicircle in the low-frequency ( $10^3$ – $10^4$  Hz) region indicates the electron-transfer resistance at the counter electrode/electrolyte ( $R_{ce}$ ) surface. The JH101–JH103-based devices contained a similar platinum counter electrode and electrolyte, and the low-frequency data gave similar  $R_{ce}$  values. The electron lifetimes ( $\tau$ ) in the  $\text{TiO}_2$  film could be extracted from the angular frequency ( $\omega_{\min}$ ) at the mid-frequency peaks of the Bode plots according to the formula  $\tau = 1/\omega_{\min}$ .<sup>33</sup> Figure 6b shows that  $\tau$  decreased in the order of JH103 > JH102 > JH101, with  $\tau = 12$ , 14, and 17 ms for the devices containing JH101–JH103, respectively. It can be noted that there is no obvious change in  $V_{oc}$  for the JH101–JH103-based devices. One reason for this phenomenon could be that the injected electrons in  $\text{TiO}_2$  are

collected effectively, implying slow recombination for each of the devices. The electron diffusion length ( $L_n$ ) is a useful tool to reflect the electron collection efficiency ( $\eta_c$ ), which can be described as  $L_n = L(R_{ct}/R_t)^{1/2}$ , where  $R_t$  represents the electron-transport resistance in the TiO<sub>2</sub> film and  $L$  is the thickness of the TiO<sub>2</sub> film (12 nm).<sup>34,35</sup>  $L_n$  values of 26.5, 24.2, and 22.5 nm can be obtained for the JH101–JH103-based devices, respectively, which are longer than the thickness of the TiO<sub>2</sub> film, implying that electron collection is efficient in all three.

The recombination and regeneration dynamics of dye<sup>+</sup> were measured by TA spectroscopy, and the detailed spectra are displayed in Figure 7. All TiO<sub>2</sub> films used for these experiments were treated with a 0.04 M TiCl<sub>4</sub> solution. The TiO<sub>2</sub> film was immersed in a dye bath with saturated CDCA for 12 h. Two electrolytes were used in these experiments: inert electrolyte A, 0.06 M LiClO<sub>4</sub> in a CH<sub>3</sub>CN solution; active electrolyte B, 0.6 M DMPII, 0.06 M LiI, and 0.04 M I<sub>2</sub> in a CH<sub>3</sub>CN solution.

The TA spectra of JH101–JH103 adsorbed on a 2- $\mu$ m-thick TiO<sub>2</sub> film and immersed in inert electrolyte A, recorded at 500 ns, are displayed in Figure 6a–c. At this time, a good signal-to-noise ratio was obtained. No bleach band was observed for the dyes at this time. The bleach was observed at 200 ns; however, at this time, the signal-to-noise ratio was weak. The absorption band from 600 to 780 nm mainly represents the absorption of dye<sup>+</sup>. The best kinetic traces for decay of this signal were obtained at 764 nm and allowed us to investigate the recombination and regeneration dynamics for JH101–JH103.

The recombination dynamics illustrated in Figure 7d–f. The absorption decay was fitted to an exponential function  $\Delta A \propto \exp[-(t/\tau)^\alpha]$ , where  $\alpha$  is the stretching parameter ( $\alpha = 1$  corresponds to a monoexponential decay) and  $\tau$  is the lifetime.<sup>31</sup>  $\tau$  values of 0.367, 0.544, and 1.16 ms can be obtained for JH101–JH103, respectively, indicating that the recombination of the injected electrons with dye<sup>+</sup> was suppressed when the number of –CH<sub>2</sub>– units was increased. We explain this trend according to nonadiabatic charge-transfer dynamics. The kinetics of recombination between the injected electrons and dye<sup>+</sup> are dependent on the spatial distance between the TiO<sub>2</sub> conduction band and the oxidized dye, which we assume to be similar in distribution to the HOMO level of neutral dye molecules.<sup>36–38</sup> We substituted inert electrolyte A for electrolyte B to evaluate the regeneration dynamics of dye<sup>+</sup>. The same fitting method as that above was undertaken. As shown in Figure 7g–i, JH103 exhibits a faster regeneration rate of 6.36  $\mu$ s compared to the other two dyes, implying that the regeneration reaction for JH103 is more efficient than those of JH101 and JH102, respectively. This trend can be explained by the electrochemical properties of the JH series of dyes. As shown in Table 1, JH101 exhibits a larger driving force of reduction compared to those of JH101 and JH102, respectively,

## CONCLUSION

In summary, a series of isoquinolinium organic dyes with different –CH<sub>2</sub>– units were synthesized and applied in DSSCs. The results indicate that the number of –CH<sub>2</sub>– units of JH101–JH103 have a small effect on the physical and electrochemical properties. However, when the dyes are applied in DSSCs,  $J_{sc}$  and the maximum IPCE of the devices incorporating JH101–JH103 decreased sharply with an increase in the number of –CH<sub>2</sub>– units. We conclude that the increased distance between the electron acceptor and TiO<sub>2</sub> does not facilitate electron injection for this series of organic

dyes. Furthermore, it is interesting to find that an increase in the number of –CH<sub>2</sub>– units can suppress the charge recombination between injected electrons with oxidized species, as evidenced by the EIS experiments. This work systematically investigated the influence of the number of –CH<sub>2</sub>– units on the physical and electrochemical properties and photovoltaic performance of DSSCs, which will pave the way for further improvements to the D– $\pi$ –A organic dyes in the future.

## ASSOCIATED CONTENT

### Supporting Information

Cyclic voltammograms and <sup>1</sup>H NMR spectra. This material is available free of charge via the Internet at <http://pubs.acs.org>.

## AUTHOR INFORMATION

### Corresponding Author

\*E-mail: [yangxc@dlut.edu.cn](mailto:yangxc@dlut.edu.cn). Tel: 0411-84986247.

### Notes

The authors declare no competing financial interest.

## ACKNOWLEDGMENTS

We gratefully acknowledge financial support of this work from the China Natural Science Foundation (Grants 21076039, 21276044, 21120102036, and 20923006), the National Basic Research Program of China (Grant 2009CB220009), the Swedish Energy Agency, K&A Wallenberg Foundation, and the State Key Laboratory of Fine Chemicals (Grant KF0805), and the Program for Innovative Research Team of Liaoning Province (Grant LS2010042).

## REFERENCES

- (1) Cai, S.; Tian, G.; Li, X.; Su, J.; Tian, H. Efficient and Stable DSSC Sensitizers Based on Substituted Dihydroindolo[2,3-*b*]carbazole Donors with High Molar Extinction Coefficients. *J. Mater. Chem. A* **2013**, *1*, 11295–11305.
- (2) Zhang, M.; Wang, Y.; Xu, M.; Ma, W.; Li, R.; Wang, P. Design of High-efficiency Organic Dyes for Titania Solar Cells Based on the Chromophoric Core of Cyclopentadithiophene-Benzothiadiazole. *Energy Environ. Sci.* **2013**, *6*, 2944–2949.
- (3) Ning, Z.; Zhang, Q.; Pei, H.; Luan, J.; Lu, C.; Cui, Y.; Tian, H. Photovoltage Improvement for Dye-Sensitized Solar Cells via Cone-Shaped Structural Design. *J. Phys. Chem. C* **2009**, *113*, 10307–10313.
- (4) Paek, S.; Cho, N.; Song, K.; Jun, M.; Lee, J. K.; Ko, J. Efficient Organic Semiconductors Containing Fluorine-Substituted Benzothiadiazole for Solution-Processed Small Molecule Organic Solar Cells. *J. Phys. Chem. C* **2012**, *116*, 23205–23213.
- (5) Zhou, J.; Zuo, Y.; Wan, X.; Long, G.; Zhang, Q.; Ni, W.; Liu, Y.; Li, Z.; He, G.; Li, C.; Kan, B.; Li, M.; Chen, Y. Solution-Processed and High-Performance Organic Solar Cells Using Small Molecules with a Benzodithiophene Unit. *J. Am. Chem. Soc.* **2013**, *135*, 8484–8487.
- (6) Zeng, W.; Cao, Y.; Bai, Y.; Wang, Y.; Shi, Y.; Zhang, M.; Wang, F.; Pan, C.; Wang, P. Efficient Dye-Sensitized Solar Cells with an Organic Photosensitizer Featuring Orderly Conjugated Ethylenedioxythiophene and Dithienosilole Blocks. *Chem. Mater.* **2010**, *22*, 1915–1925.
- (7) Tian, H.; Yang, X.; Chen, R.; Zhang, R.; Hagfeldt, A.; Sun, L. Effect of Different Dye Baths and Dye-Structures on the Performance of Dye-Sensitized Solar Cells Based on Triphenylamine Dyes. *J. Phys. Chem. C* **2008**, *112*, 11023–11033.
- (8) Hagberg, D. P.; Edvinsson, T.; Marinado, T.; Boschloo, G.; Hagfeldt, A.; Sun, L. A Novel Organic Chromophore for Dye-Sensitized Nanostructured Solar Cells. *Chem. Commun.* **2006**, *21*, 2245–2247.

- (9) Kitamura, T.; Ikeda, M.; Shigaki, K.; Inoue, T.; Anderson, N. A.; Ai, X.; Lian, T.; Yanagida, S. Phenyl-Conjugated Oligoene Sensitizers for TiO<sub>2</sub> Solar Cells. *Chem. Mater.* **2004**, *16*, 1806–1812.
- (10) Karlsson, K. M.; Jiang, X.; Eriksson, S. K.; Gabrielsson, E.; Rensmo, H.; Hagfeldt, A.; Sun, L. Phenoxazine Dyes for Dye-Sensitized Solar Cells: Relationship Between Molecular Structure and Electron Lifetime. *Chem.—Eur. J.* **2011**, *17*, 6415–6424.
- (11) Horiuchi, T.; Miura, H.; Sumioka, K.; Uchida, S. High Efficiency of Dye-Sensitized Solar Cells Based on Metal-Free Indoline Dyes. *J. Am. Chem. Soc.* **2004**, *126*, 12218–12219.
- (12) Ito, S.; Zakeeruddin, S. M.; Baker, R. H.; Liska, P.; Charvet, R.; Comte, P.; Nazeeruddin, M. K.; Pechy, P.; Takata, M.; Miura, H.; Uchida, S.; Grätzel, M. High-Efficiency Organic-Dye-Sensitized Solar Cells Controlled by Nanocrystalline-TiO<sub>2</sub> Electrode Thickness. *Adv. Mater.* **2006**, *18*, 1202–1205.
- (13) He, J.; Guo, F.; Li, X.; Wu, W.; Yang, J.; Hua, J. New Bithiazole-Based Sensitizers for Efficient and Stable Dye-Sensitized Solar Cells. *Chem.—Eur. J.* **2012**, *18*, 7903–7915.
- (14) Liu, B.; Wang, R.; Mi, W.; Li, X.; Yu, H. Novel Branched Coumarin Dyes for Dye-Sensitized Solar Cells: Significant Improvement in Photovoltaic Performance by Simple Structure Modification. *J. Mater. Chem.* **2012**, *22*, 15379–15387.
- (15) Chang, D. W.; Lee, H. J.; Kim, J.; Park, S. Y.; Park, S. M.; Dai, L.; Baek, J. B. Novel Quinoxaline-Based Organic Sensitizers for Dye-Sensitized Solar Cells. *Org. Lett.* **2011**, *13*, 3880–3883.
- (16) Do, K.; Kim, D.; Cho, N.; Paek, S.; Song, K.; Ko, J. New Type of Organic Sensitizers with a Planar Amine Unit for Efficient Dye-Sensitized Solar Cells. *Org. Lett.* **2012**, *14*, 222–225.
- (17) Tian, H.; Bora, I.; Jiang, X.; Gabrielsson, E.; Karlsson, K. M.; Hagfeldt, A.; Sun, L. Modifying Organic Phenoxazine Dyes for Efficient Dye-Sensitized Solar Cells. *J. Mater. Chem.* **2011**, *21*, 12462–12472.
- (18) Tian, H.; Yang, X.; Chen, R.; Zhang, R.; Hagfeldt, A.; Sun, L. Effect of Different Dye Baths and Dye-Structures on the Performance of Dye-Sensitized Solar Cells Based on Triphenylamine Dyes. *J. Phys. Chem. C* **2008**, *112*, 11023–11033.
- (19) Zhang, J.; Yao, Z.; Cai, Y.; Yang, L.; Xu, M.; Li, R.; Zhang, M.; Dong, X.; Wang, P. Conjugated Linker Correlated Energetics and Kinetics in Dithienopyrrole Dye-Sensitized Solar Cells. *Energy Environ. Sci.* **2013**, *6*, 1604–1614.
- (20) Tsao, H. N.; Yi, C.; Moehl, T.; Yum, J. H.; Zakeeruddin, S. M.; Nazeeruddin, M. K.; Grätzel, M. Cyclopentadithiophene Bridged Donor–Acceptor Dyes Achieve High Power Conversion Efficiencies in Dye-Sensitized Solar Cells Based on the *tris*-Cobalt Bipyridine Redox Couple. *ChemSusChem* **2011**, *4*, 591–594.
- (21) Tian, H.; Yang, X.; Cong, J.; Chen, R.; Liu, J.; Hao, Y.; Hagfeldt, A.; Sun, L. Tuning of Phenoxazine Chromophores for Efficient Organic Dye-Sensitized Solar Cells. *Chem. Commun.* **2009**, *45*, 6288–6290.
- (22) Zhao, J.; Yang, X.; Cheng, M.; Li, S.; Wang, X.; Sun, L. Highly Efficient *Iso*-quinoline Cationic Organic Dyes without Vinyl Groups for Dye-Sensitized Solar Cells. *J. Mater. Chem. A* **2013**, *1*, 2441–2446.
- (23) Teng, C.; Yang, X.; Yang, C.; Li, S.; Cheng, M.; Hagfeldt, A.; Sun, L. Molecular Design of Anthracene-Bridged Metal-Free Organic Dyes for Efficient Dye-Sensitized Solar Cells. *J. Phys. Chem. C* **2010**, *114*, 9101–9110.
- (24) Ziolk, M.; Yang, X.; Sun, L.; Douhal, A. Interrogating the Ultrafast Dynamics of an Efficient Dye for Sunlight Conversion. *Phys. Chem. Chem. Phys.* **2010**, *12*, 8098–8107.
- (25) Yang, C. J.; Chang, Y. J.; Watanabe, M.; Hon, Y. S.; Chow, T. J. Phenothiazine Derivatives as Organic Sensitizers for Highly Efficient Dye-Sensitized Solar Cells. *J. Mater. Chem.* **2012**, *22*, 4040–4049.
- (26) Kim, S.; Choi, H.; Kim, D.; Song, K.; Kang, S. O.; Ko, J. Novel Conjugated Organic Dyes Containing Bis-dimethylfluorenyl Amino Phenyl Thiophene for Efficient Solar Cell. *Tetrahedron* **2007**, *63*, 9206–9212.
- (27) Sayama, K.; Hara, K.; Mori, N.; Satsuki, M.; Suga, S.; Tsukagoshi, S.; Abe, Y.; Sugihara, H.; Arakawa, H. Photosensitization of a Porous TiO<sub>2</sub> Electrode with Merocyanine Dyes Containing a Carboxyl Group and a Long Alkyl chain. *Chem. Commun.* **2000**, *13*, 1173–1174.
- (28) Hara, K.; Sato, T.; Katoh, R.; Furube, A.; Yoshihara, T.; Murai, M.; Kurashige, M.; Ito, S.; Shinpo, A.; Suga, S.; Arakawa, H. Novel Conjugated Organic Dyes for Efficient Dye-Sensitized Solar Cells. *Adv. Funct. Mater.* **2005**, *15*, 246–252.
- (29) Boschloo, G.; Hagfeldt, A. Activation Energy of Electron Transport in Dye-Sensitized TiO<sub>2</sub> Solar Cells. *J. Phys. Chem. B* **2005**, *109*, 12093–12098.
- (30) Morandeira, A.; López-Duarte, I.; Martínez-Díaz, M.; O'Regan, B.; Shuttle, C.; Haji-Zainulabidin, N. A.; Torres, T.; Palomares, E.; Durrant, J. R. Slow Electron Injection on Ru–Phthalocyanine Sensitized TiO<sub>2</sub>. *J. Am. Chem. Soc.* **2007**, *129*, 9250–9251.
- (31) Kroeze, J. E.; Hirata, N.; Koops, S.; Nazeeruddin, M. K.; Schmidt-Mende, L.; Grätzel, M.; Durrant, J. R. Alkyl Chain Barriers for Kinetic Optimization in Dye-Sensitized Solar Cells. *J. Am. Chem. Soc.* **2006**, *128*, 16376–16383.
- (32) Wang, Z.; Koumura, N.; Cui, Y.; Takahashi, M.; Sekiguchi, H.; Mori, A.; Kubo, T.; Furube, A.; Hara, K. Hexylthiophene-Functionalized Carbazole Dyes for Efficient Molecular Photovoltaics: Tuning of Solar-Cell Performance by Structural Modification. *Chem. Mater.* **2008**, *20*, 3993–4003.
- (33) Pei, K.; Wu, Y.; Wu, W.; Zhang, Q.; Chen, B.; Tian, H.; Zhu, W. Constructing Organic D–A– $\pi$ -A-Featured Sensitizers with a Quinoxaline Unit for High-Efficiency Solar Cells: The Effect of an Auxiliary Acceptor on the Absorption and the Energy Level Alignment. *Chem.—Eur. J.* **2012**, *18*, 8190–8200.
- (34) Bandi, Z. Z.; Bridger, P. M.; Piquette, E. C.; McGill, T. C. Electron Diffusion Length and Lifetime in P-type GaN. *Appl. Phys. Lett.* **1998**, *73*, 3276–3278.
- (35) Kuang, D.; Ito, S.; Wenger, B.; Klein, C.; Moser, J.; Humphry-Baker, R.; Zakeeruddin, S. M.; Grätzel, M. High Molar Extinction Coefficient Heteroleptic Ruthenium Complexes for Thin Film Dye-Sensitized Solar Cells. *J. Am. Chem. Soc.* **2006**, *128*, 4146–4154.
- (36) Haque, S. A.; Tachibana, Y.; Willis, R. L.; Moser, J. E.; Grätzel, M.; Klug, D. R.; Durrant, J. R. Parameters Influencing Charge Recombination Kinetics in Dye-Sensitized Nanocrystalline Titanium Dioxide Films. *J. Phys. Chem. B* **2000**, *104*, 538–547.
- (37) Ardo, S.; Meyer, G. Photodriven Heterogeneous Charge Transfer with Transition-metal Compounds Anchored to TiO<sub>2</sub> Semiconductor Surfaces. *Chem. Soc. Rev.* **2009**, *38*, 115–164.
- (38) Pastore, M.; Angelis, F. D. Computational Modelling of TiO<sub>2</sub> Surfaces Sensitized by Organic Dyes with Different Anchoring Groups: Adsorption Modes, Electronic Structure and Implication for Electron Injection/Recombination. *Phys. Chem. Chem. Phys.* **2012**, *14*, 920–928.